Chapter 6

Radio Wave Propagation Through Vegetation

Mir Ghoraishi, Jun-ichi Takada and Tetsuro Imai

Additional information is available at the end of the chapter

http://dx.doi.org/10.5772/52571

1. Introduction

Vegetation is an indispensable feature of most outdoor wireless channel environments. The interaction between radio waves and vegetation has been researched for several decades. Because of the complex structure of the foliage, composed of randomly oriented trunks, branches, twigs and leaves, the involved physical process in the propagation of the radio wave through vegetation is complex. Accurate modeling of the propagation of radio waves through tree foliage, generally requires accurate electromagnetic description of the tree geometry, including its branches and leaves, valid over a wide range of frequencies. Originally empirical models were developed to describe the propagation of radio waves in the vegetation. In other approaches this interaction is analyzed using ray-based techniques. More recently theoretical –statistical and analytical– approaches became favorable. As it is discussed in the next section, major disadvantage of all these models is that the final outcome is basically presented by providing an excess attenuation to that caused by free space propagation.

1.1. Existing approaches

Empirical models have been developed to characterize the the propagation of radio waves in the vegetation for years. Their significant advantage is their simplicity. The drawback is that, like any other empirical model, the formulated model is strictly related to the specific measured data set and fails to give any indication as to the physical processes involved in the propagation within the channel. These models usually provide either the mean attenuation of the propagation signal caused by vegetation or calculate the link budget. Parameters in these models, e.g. frequency, incident angles, direct-path length through vegetation and other parameters associated with the specific environment under which measurements were performed, are usually computed through regression curves fitted to measurement data. Among many, the modified exponential decay model suggested in [1], and the COST 235 model [2] can be mentioned. These models are expressed as equations in exponential forms to give the specific attenuation as a function of path length and operating frequency. The attenuation of trees as a function of vegetation depth has been shown to be more accurately represented by dual slope attenuation functions [3]-[7]. To accommodate this dual slope, an

empirical nonzero gradient model was developed to follow the dual gradient of the measured attenuation curve [8]. The initial slope describes the loss experienced by the coherent component, whereas the second slope describes the dominance of the incoherent component, which occurs at a much reduced rate. An important disadvantage of the semi-empirical vegetated radio channel models, common to other approaches such as radiative transfer theory, is that their little account of the dynamic effects in the channel and no account of the wideband effects of the vegetation medium.

Another approach in the the analysis and prediction of the vegetated radio channel is ray-tracing [9]-[16]. These have to be carefully designed and used, taking into account the frequency of the radio wave, the dimension of interacting objects and their distance to the sources to fulfill the far field condition. Therefore in different frequencies the mechanisms by which the wave propagates can vary dramatically. The scattering has been modeled deterministically in many different ways depending on the electrical density of the vegetative medium. At lower frequencies, where individual components of the vegetation (trunks, branches, twigs and leaves or needles) and their separations are small by comparison with the radio wavelength, considering the vegetation as a homogeneous dielectric slab, the propagation has been modeled in terms of a lateral wave at treetop heights [9]. At frequencies above 200 [MHz] or so, a single slab becomes inadequate. As the scale of the changes in density and structure of the vegetation become greater than the order of a wavelength, and layered representations of the vegetation should be used [10]. A full-wave analysis of the radiowave propagating along mixed paths inside a four-layered forest model applicable to frequencies up to 3 [GHz] was proposed in [11], [12], which consists of four isotropic and homogeneous dielectric. The first layer is the semi-infinite free-space, whereas the second layer represents the forest canopy. The third and fourth layers model the trunk and the semi-infinite ground plane, respectively. As the distance between the transmitter and the receiver is very long, the radio wave propagation through the stratified forest is characterized by the lateral wave that mainly propagates on top of the canopy along the air-canopy interface. For short distances, however, such a propagation is denominated by the direct or coherent component. When the receiver is at a clearing distance from the dense vegetated area the edge of the forest is treated as a source of diffraction [14], and the uniform theory of diffraction (UTD) associating a double-diffracted component over the canopy and a transmission component which includes the exact calculation of refraction angles is also used [15].

To model the incoherent component which is the dominant propagation mechanism for long distances inside vegetation, theoretical models, which are more complicated but more generic and applicable to any arbitrary foliage wave propagation scenario, are used. Two major approaches, namely the radiative transfer theory and the analytical theory, have been pursued to develop these models [17],[18]. These two methods are closely related as they are addressing the same problem of the wave propagation in randomly distributed particles. In fact, the radiative transfer theory can be derived from analytical approach by applying some approximations [17], and they have proven equivalent for the application of radar in the forest canopies [19].

In the method of radiative transfer theory, the vegetation medium is modeled as a statistically homogeneous random medium of scatterers which is characterized by parameters such as the absorption cross-section per unit volume, the scatterer cross-section per unit volume and the scattering function of the medium [20]. The scattering function (phase function) is

characterized by a narrow forward lobe and an isotropic background. The model considers a plane wave incident from an air half space upon the planar interface of a vegetation half space. The basic equation of the radiative energy transfer theory is expressed in terms of the specific intensity for which the radiative transfer theory gives the specific value at a given point within the vegetation medium as a sum of a coherent component and an incoherent component. The coherent component is reduced in intensity due to absorption and scattering of the incident wave, and the incoherent component due to the scattered wave. Each scatterer is assumed to have a directional scattering profile, or phase function. As the constituents of the tree are relatively large compared to the wavelength at micro- and millimeter wave frequencies, the scattering function is assumed to consist of a strongly scattering forward lobe, which can be assumed to be Gaussian with an isotropic background level. The radiative transfer theory predicts the dual slope nature of the measured attenuation versus vegetation depth curves and provides a physical interpretation. The equation based on the radiative transfer theory allows the prediction of the attenuation curves in which the received signal is reduced linearly by scattering and absorption of the incident signal. As the receiver is moved deeper into the vegetation, and the direct coherent component is reduced further still, the isotropically scattered component becomes significant. Due to the increase of scattering volume as we move deeper into the medium, the scattering signal level tends to be maintained, leading in turn to an attenuation rate which is significantly reduced at these depths. The model however requires four input parameters namely the ratio of the forward scattered power to the total scattered power, the beam-width of the phase function, the combined absorption and scattering coefficient, and the albedo. These are extracted from path-loss measurement data so that the approach makes itself a semi-empirical model in essence. Direct computation of these parameters, such as the albedo and the phase function, is very difficult, because the vertical profile of the foliage is inhomogeneous, i.e. the distinction exists between the trunk layer and the crown layer, whereas the radiative transfer approach is generally applied to a homogeneous medium. In order to overcome this limitation, an improved version of the discrete radiative transfer is proposed for isolated vegetation specimens [21],[22]. However this requires discretization of the foliage into small cells which is numerically intractable for large propagation distances.

The alternative approach in the problem of wave propagation in randomly distributed particles is the analytical approach [17]. This is usually in the format of Foldy-Lax solution for point scatterers [18],[23], which has been widely used to estimate the signal attenuation in the the foliage [24]-[32]. In this approach the Born approximation is applied to account only the first term in the equation as considering higher terms can complicate the computations prohibitively [18]. It predicts the exponential decay of the radio field corresponding to the linear foliage path-loss (in dB) versus the wave propagation distance. In [24]-[30], the inhomogeneous forest structure was represented by using a realistic-looking fractal tree model. The statistics of the received field are then obtained through a Monte Carlo technique which generates random forest structures according to prescribed statistical botanical features, such as tree height, branch and leaf orientation angles, and tree locations. Another approach is to model leaves as flat circular lossy dielectric discs, and branches as finitely long circular lossy dielectric cylinders [31],[32]. The disadvantage of the analytical approach stems from the fact that Born approximation accounts only for single scattering, which has been shown to overestimate the foliage path-loss at high frequencies or over long distance propagation where the multiple-scattering effects become important [28],[29]. Another concern with this method is the required computation time. Computing foliage

path-loss over long distances in a forested environment can be prohibitively time-consuming even with the single-scattering model. This difficulty can be circumvented by treating the forest as a statistically homogeneous medium along the direction of wave propagation and only analyzing the wave propagation behaviors in a typical block of forest, which can then be reused for all forest blocks [30]. Furthermore a main concern in Born approximation is its validity is restricted to scatterers with a dielectric permittivity close to unity and that the effect of multiple scattering from the discrete scatterers are not negligible [33]. To overcome these limitations the Feynman diagrams are converted to the set of expanded green functions presented in integral operator form is suggested as an alternative to Born approximation [33],[34].

To benefit from the ray-tracing and theoretical approaches at the same time, the model proposed in [35] combines the effects of three individual propagation modes, i.e. diffraction from the side and top of the foliage, ground reflection and direct (through vegetation) propagation. In this approach the extent of the vegetation is modeled as rectangular hexahedrons (boxes). The loss experienced by the diffracted waves over the vegetation as well as those around the vegetation are treated as double isolated knife-edge diffraction. If the ground reflection is passed through vegetation, the path loss due to propagation through vegetation is added to the reflection loss. The values for the permittivity and conductance of the ground are obtained from ITU-R recommendations [36]. For the direct through vegetation propagation component the radiative transfer approach is adopted and the necessary parameters for specific geometries, species and frequencies are measured and provided in tables [35]. This model was adopted by ITU-R and later works published as recommendations of ITU-R have improved the tables of parameters for some kind of trees [37].

While the above mentioned models mostly ignore the channel dynamics over time, narrowband analysis of the wind effect on an isolated tree in the anechoic chamber is reported in [38]-[40].

1.2. Directional analysis of the vegetation radio channel

Either if the interaction between radio signal and foliage is modeled based on diffraction theories and ray-tracing, radiative transfer theory, analytical theory, statistical, or empirical approaches, it is usually aimed to provide an excess attenuation to that caused by free space propagation. On the other hand, as these models are strongly dependent on measurements for their evaluation and modifications, a considerable number of experiments have been accomplished to analyze the foliage influence on the propagation channel as well as to evaluate the proposed models. The ultimate target in most of these experiments however is to measure the attenuation of the radio wave caused by the vegetation. The problem is that even though such a result proves useful for specific purposes, it provides only limited knowledge about the interactions in the channel. On the other hand, the assumption of homogeneous media of randomly distributed scattering points is widely used in analytical and statistical approaches, an assumption to be examined yet. Obviously with a high-resolution spatial analysis of the vegetation radio channel, the existing methods and their assumptions can be further evaluated and if necessary modified. Moreover, such an analysis can be used in design and performance analysis of modern wireless systems equipped with multiple-antenna

technologies to improve the capacity. Never the less, and in spite of such significant benefits, such measurements and analyses are rarely reported due to practical limitations.

Few recent reports address –indirectly in most cases– the spatial characteristics of the radio channel in vegetation. The delay power spectrum of the received signal through a single isolated tree for different angle-of-incidents is evaluated for a wideband signal in [41]. The spatial correlation of a multiple antenna system operated in the forest is evaluated in [42]. The scattering effect of the foliage in suburban scenarios is examined by directive antennas [43], and delay spread of the received signal as a result of scattering by trees was observed [44]. In a recent publication, the delay and angular spread of the wireless channel for the application in positioning of mobile users is reported [45].

In this chapter the directional radio channel in dense vegetation is investigated. An experimental approach is necessary because of the complexity of the underlying phenomena. The methodology used for this purpose, is the directional analysis of a carefully captured measurement data. First the measurement campaign and setup parameters as well as the signal model are introduced in section 2, and then two analysis methods for the measured data are discussed. In the first approach, the experimental data is analyzed by calculating the received signal dispersion in delay and azimuth-of-arrival of the propagated waves which is done using a Capon beam-forming technique [46]. One advantage of such analysis is that no presumption on the distribution of the dispersed signal was necessary. In the second approach, a high-resolution parameter estimation technique was adopted to acquire a more accurate knowledge of the channel, particularly to identify the involving propagation mechanisms. Results of the analysis by each method, including the multipath cluster identification and propagation mechanism determination are presented in section 3. Section 4 provides discussions on the findings of the chapter, the analysis and results, and argues how the directional analysis, aiming at the identification of dominant propagation mechanisms in the channel, can meaningfully improve the insight toward the problem. Section 5 sums up important conclusions of the chapter.

2. Method

2.1. Experimental investigation

As it was expressed, to clarify the influence of the vegetation on the radio channel, and specifically to re-examine those fundamental assumptions usually presumed in such studies we had to gather a set of experimental data with necessary resolution in delay and spatial domains. For this propose a dense vegetated area was chosen in the southern Kanagawa, Japan. A schematic of the measurement scenario is illustrated in Fig. 1 where the height of the base-station antenna could be altered and the mobile-station antenna height is fixed. The employed channel sounder is a double-directional sounder at the center frequency of 2.22 [GHz]. The sounder specifications and the measurement set-up parameters are found in Table 1. At the transmitter a sleeve and a slot antenna are used to send the vertically and horizontally polarized signal in different time slots. The cylindrical array antenna at the receiver switches the vertical and horizontal patch antenna feeds, 96 elements for each polarizations. The transmitter antennas are mounted on a measurement bucket capable to elevate up to 15 [m]. Measurements were performed on the 4, 6, 9, 12 and 15 [m] of the transmitter antenna heights. The receiver antenna array is installed on the roof-top of a

f_c	2.22 [GHz]
Tx signal	OFDM, 2048 FFT points
Number of subcarrier	897
Tx signal bandwidth	50 MHz
Tx power	30 [dBm]
Tx antenna	sleeve, slot (different time slots)
Tx antenna height	15, 12, 9, 6, 4 [m]
Rx antenna	Cylindrical array (4 ring stacked) 96 elements V/H
Rx antenna height	3.5 [m] (installed on the van's roof-top)
Tx-Rx separation	100 [m]
Tallest trees height	10 [m]

Table 1. Specifications of Experiment

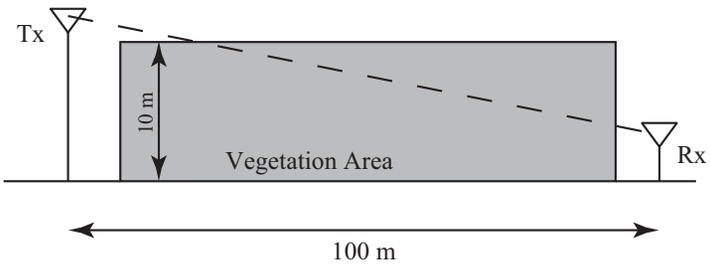

Figure 1. Measurement scenario.

measurement van which carries the receiver system. The van is parked deep in the vegetation area with a transmitter to receiver horizontal distance of about 100 [m]. Here we only report the static channel that is the measurement van has been parked during the measurement. The tallest trees are mostly Japanese cedar whereas in lower layers of the vegetation several kinds of trees are found as it can be seen in Fig. 2. No significant scattering other than trees is observable around the receiver.

With such a measurement setup we are able to achieve a more accurate analysis of the radio channel. Two different analysis methods are introduced in next sections and then the interpretations are compared.

2.2. Analysis approaches

A major part of the reported experiments regarding the interaction of radio with vegetations targeting the spatial analysis use directional antennas or an array antenna with beam-forming scheme. A good reason for this is the simplicity of such measurements, compared to more complicated ones concluding in high-resolution analysis. An important but less obvious reason is that since in case of propagation through vegetation we know little about the distribution of effective scatterers, beam-forming as a robust approach seems the appropriate candidate for the analysis. This is expressed in contrast to the model based estimation methods although the resolution of the beam-forming is inferior. In this section two methods

Figure 2. Different types of trees in the foliage.

for the analysis of the measurement data are presented. First we introduce a Capon beam-former to analyze and provide the spread of the received radio signals. In the next step a high-resolution SAGE algorithm is introduced for the analysis of the multidimensional measurement data.

2.2.1. Signal model

Assuming multipath in the channel, the signal observed at the output of the receiver array can be represented in vector notation as [48]

$$\begin{aligned}\mathbf{Y}(t) &\doteq [Y_1(t), \cdots, Y_{N_\mathrm{r}}(t)]^\mathrm{T} \\ &= \sum_{l=1}^{L} \mathbf{s}(t;\boldsymbol{\theta}_l) + \sqrt{\frac{N_0}{2}}\mathbf{w}(t),\end{aligned} \tag{1}$$

where $\mathbf{Y}(t)$ is the N_r dimensional vector of received signals at the receiver array with N_r antenna elements and $\mathbf{s}(t;\boldsymbol{\theta}_l)$ is the contribution of the lth multipath to the received signal, again a vector with N_r elements and it is assumed that L multipath are successfully received by the receiver. The N_r dimensional complex, temporally and spatially white noise is denoted by $\mathbf{w}(t)$ and N_0 is a positive constant.

The parametric characteristic of the lth propagation wave is described by vector $\boldsymbol{\theta}_l$ which is represented for the current directional and polarimetric measurement as

$$\boldsymbol{\theta}_l \doteq [\boldsymbol{\Omega}_{\mathrm{r}l}, \tau_l, \mathbf{A}_l]. \tag{2}$$

Here the subscript '$_l$' indicates the correspondence to the lth path and the parameters are angle-of-arrival $\boldsymbol{\Omega}_{\mathrm{r}l} = [\varphi_{\mathrm{r}l}, \vartheta_{\mathrm{r}l}]$ with $\varphi_{\mathrm{r}l}$ indicating the azimuth-of-arrival for the propagation wave calculated in degrees, counter clockwise with its origin along the direction of receiver toward the transmitter, and $\vartheta_{\mathrm{r}l}$ being the elevation-of-arrival of the propagation wave computed in degrees from the horizon with increasing values upward, so called coelevation.

Other parameters are excess-delay τ_l and complex magnitude $\mathbf{A}_l$ is the vector to represent the weights for the co- and cross-polarization components according to

$$\mathbf{A}_l \doteq \begin{bmatrix} \alpha_{\mathrm{v}l} \\ \alpha_{\mathrm{h}l} \end{bmatrix}. \tag{3}$$

It is observed that due to the static measurement scenario Doppler-frequency of the propagation multipath is not considered, otherwise its value is expected to be zero or negligible. The contribution of the lth multipath to the received signal can therefore be expressed in vector notation as

$$\begin{aligned} \mathbf{s}(t;\boldsymbol{\theta}_l) &\doteq [s_1(t;\boldsymbol{\theta}_l), \cdots, s_{N_\mathrm{r}}(t;\boldsymbol{\theta}_l)]^{\mathrm{T}} \\ &= \mathbf{C}_\mathrm{r}(\boldsymbol{\Omega}_{\mathrm{r}l})\mathbf{A}_l u(t-\tau_l). \end{aligned} \tag{4}$$

The matrix $\mathbf{C}_\mathrm{r}(\boldsymbol{\Omega})$ in (4) is defined as $\mathbf{C}_\mathrm{r}(\boldsymbol{\Omega}) \doteq [\mathbf{c}_{\mathrm{rv}}(\boldsymbol{\Omega}), \mathbf{c}_{\mathrm{rh}}(\boldsymbol{\Omega})]$ (v and h subscripts indicate V- and H-polarizations) where the N_r dimensional-vector receiver array radiation pattern for the propagation wave impinging from direction $\boldsymbol{\Omega}_{\mathrm{r}l} = [\varphi_{\mathrm{r}l}, \vartheta_{\mathrm{r}l}]$ at the receiver is denoted as $\mathbf{c}_{\mathrm{r}p_\mathrm{r}}(\boldsymbol{\Omega}_{\mathrm{r}l})$ and is defined as

$$\mathbf{c}_{\mathrm{r}p_\mathrm{r}}(\boldsymbol{\Omega}) \doteq [f_{n_\mathrm{r},p_\mathrm{r}}(\boldsymbol{\Omega}) \exp\{j2\pi\lambda^{-1}\boldsymbol{\Omega}\cdot\mathbf{r}_{n_\mathrm{r}}\}]; \quad n_\mathrm{r} = 1, \cdots, N_\mathrm{r}]^{\mathrm{T}}, \tag{5}$$

for the receiver polarization $p_\mathrm{r} \in \{\mathrm{v}, \mathrm{h}\}$ and $f_{n_\mathrm{r},p_\mathrm{r}}(\boldsymbol{\Omega})$ denotes the radiation pattern for the n_rth element of the array. The transmitted signal at any arbitrary time instance t is an impulse train in the frequency domain which is obtained as

$$u(t) = \sum_{b=-B}^{B} \delta(f_\mathrm{c} + bf_\mathrm{s}), \tag{6}$$

where f_c is the center frequency of the sounding signal, f_s is the DFT frequency shift and the signal bandwidth is therefore equal to $(2B+1)f_\mathrm{s}$. The energy of the signal is assumed as P. A delayed version of such a signal is represented as

$$u(t-\tau) = e^{-j2\pi f_\mathrm{s}\tau}\, u(t). \tag{7}$$

Thus the signal model (4) can be represented as

$$\mathbf{s}(t;\boldsymbol{\theta}_l) = e^{-j2\pi f_\mathrm{s}\tau_l}\, \mathbf{C}_\mathrm{r}(\boldsymbol{\Omega}_{\mathrm{r}l})\, \mathbf{A}_l\, u(t). \tag{8}$$

It is assumed that each snapshot of the sounding signal is transmitted during T_s (sounding signal duration), in I consecutive intervals each longer than transmitted signal duration.

2.2.2. Beam-forming

Capon beam-former, or minimum variance distortionless response (MVDR) beam-former, is proved optimum for estimating an unknown random plane-wave signal, being received in the presence of noise, to provide a minimum variance unbiased estimate [49]. This is equivalent to passing the signal through a distortionless filter which minimizes the output variance. A significant advantage of this algorithm when used in the parameter estimation context is that the provided spatial spectral estimate does not rely on any underlying signal model [49]. The approach employed in this section was previously used to estimate the azimuth of

the distributed source components in [50]. Following the same method, the first and second moments of the azimuth-of-arrival and excess-delay spread of the received radio waves are calculated.

We consider the directional but stationary scenario where the L multipath are received in D_m received signal clusters at each measurement m (at each specific transmitter antenna height) as

$$\mathbf{Y}_m(t) = \sum_{d=1}^{D_m} \sum_{l \in \mathrm{C}_{m,d}} \mathbf{s}(t; \boldsymbol{\theta}_l) + \sqrt{\frac{N_0}{2}} \mathbf{w}(t), \qquad m = 1, \cdots, M\,, \tag{9}$$

where $\mathrm{C}_{m,d}$ is the set of multipath in dth cluster of mth measurement. It is observed that the definition of cluster is dependent to the resolution of the analysis scheme. Hence in the next section where high-resolution algorithm is used, a distinct definition for the multipath cluster is employed. Furthermore, in the beam-forming analysis of the signal we neglect the elevation-of-arrival ϑ_r of the received signal because of low resolution of the analysis in this dimension and therefore the propagation in azimuth plane only is considered. In the current analysis although the resolution is not enough to separate multipath, but the delay spread is already available by performing the inverse discrete Fourier transform on the measured data samples with the resolution $\tau_\mathrm{res} = ((2B+1)f_\mathrm{s})^{-1}$ and the azimuth-power spectrum at each delay is computed by a Capon beam-forming due to its better resolution in comparison to the conventional approach. The Capon spectrum is obtained as [49]:

$$P_m(\varphi_\mathrm{r}, \tau_k)\Big|_{p_\mathrm{t}p_\mathrm{r}} = \frac{1}{\mathbf{c}^\mathrm{H}_{\mathrm{r}p_\mathrm{r}}(\varphi_\mathrm{r}, 0)\, \mathbf{R}^{-1}_{\mathbf{Y}_{mp_\mathrm{t}}}(\tau_k)\, \mathbf{c}_{\mathrm{r}p_\mathrm{r}}(\varphi_\mathrm{r}, 0)}\,, \tag{10}$$

where $\mathbf{R}_{\mathbf{Y}_{mp_\mathrm{t}}}$ is the received signal covariance matrix for the measurement m and transmitter antenna polarization of p_t, $\mathbf{c}_{\mathrm{r}p_\mathrm{r}}(\varphi_\mathrm{r}, 0)$ is the receiver array response in the azimuth plane for the polarization p_r and $\tau_k = (k-1)\tau_\mathrm{res}$ is a specific delay within the range. Figure 3 presents a sample of computed delay-azimuth-power spectrum for the transmitter antenna height of 15 [m] ($m = 1$), where the transmitted signal and the receiving antenna feeds are in vertical polarization ($p_\mathrm{t}p_\mathrm{r} = \mathrm{vv}$). The figure indicates –and it is the case for most measured data in this campaign– that the radio signal is received as a cluster of multipath with probably a Gaussian or von-Mises spread in the azimuth, and an exponential spread along the delay. We therefore modify the signal model to $D_m = 1$ for all values of m and drop the index d in the beam-forming data analysis. In the analysis the normalized spectrum $\dot{P}_m(\varphi_\mathrm{r}, \tau)$ to the minimum value of the spectrum within a support around the considered multipath cluster is used which is calculated for each measurement m at polarization combination $p_\mathrm{t}p_\mathrm{r}$. The size of the support shall be selected large enough to include the diffuse components but not so large to have any multipath from other clusters in. It is noticed however that in a beam-forming approach the array antenna response could not be de-embedded from the measured data. Another disadvantage is low spatial resolution resulting in the single cluster presumption.

2.2.3. High-resolution parameter estimation

A space-alternative generalized EM algorithm (SAGE) was employed to estimate the vector of parameters $\boldsymbol{\theta}_l$ for each propagation wave within the resolution of the system [51]. Observation of the estimated paths indicates a large cross polarization ratio in most cases and therefore the results presented here does not discuss the cross polarization of the multipath. Thus

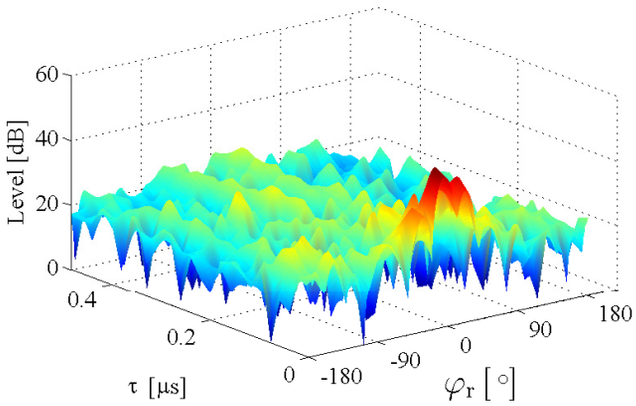

Figure 3. delay-azimuth-power spectrum of the received waves for transmitter antenna height of 15 m, VV case.

the subscript indicating the polarization of the complex magnitude $\alpha_{p_r l}$, i.e. $p_r \in \{v,h\}$, is dropped in further discussions.

Several tens of multipath are detected at each measurement points, while this number could reach well beyond 100 in a couple of measurements. The array calibration indicates that array response for extreme elevation-of-arrival values is highly unreliable. Hence we have neglected those estimated multipath impinging with too high or too low elevation-of-arrival, i.e. we consider the acceptable range of elevation-of-arrival as $\vartheta_{rl} \in (-75°, 75°)$.

3. Analysis

3.1. Moments of radio wave spread –beam-forming

Having the delay-azimuth-power spectrum of the measured data computed we can obtain the mean values $\bar{\varphi}_m$ and $\bar{\tau}_m$, and the standard deviations σ_{φ_m} and σ_{τ_m} for each measurement m simply as:

$$\bar{\varphi}_m(\tau_k) = \frac{\sum_{\varphi_r \in \Phi} \varphi_r \dot{P}_m(\varphi_r, \tau_k)}{\sum_{\varphi_r \in \Phi} \dot{P}_m(\varphi_r, \tau_k)}, \tag{11}$$

$$\sigma_{\varphi_m}(\tau_k) = \left(\frac{\sum_{\varphi_r \in \Phi} (\varphi_r - \bar{\varphi}_r)^2 \dot{P}_m(\varphi_r, \tau_k)}{\sum_{\varphi_r \in \Phi} \dot{P}_m(\varphi_r, \tau_k)} \right)^{1/2}, \tag{12}$$

$$\bar{\tau}_m(\varphi_{rq}) = \frac{\sum_{\tau \in \Xi} \tau_k \dot{P}_m(\varphi_{rq}, \tau)}{\sum_{\tau \in \Xi} \dot{P}_m(\varphi_{rq}, \tau)}, \tag{13}$$

$$\sigma_{\tau_m}(\varphi_{rq}) = \left(\frac{\sum_{\tau \in \Xi} (\tau - \bar{\tau})^2 \dot{P}_m(\varphi_{rq}, \tau)}{\sum_{\tau \in \Xi} \dot{P}_m(\varphi_{rq}, \tau)} \right)^{1/2}, \tag{14}$$

where $\Xi = \{0, \tau_{res}, \cdots, T_s\}$, $\Phi = \{-\varphi_{max}, \cdots, -\varphi_{res}, 0, \varphi_{res}, \cdots, \varphi_{max}\}$, with φ_{res} being the sampling resolution of the beam-forming.

The mean and standard deviation values of the excess-delay and azimuth-of-arrival for the direct path, $\bar{\varphi_m}|_{\tau_k=0}$, $\bar{\tau_m}|_{\varphi_q=0}$, $\sigma_{\tau_m}|_{\varphi_q=0}$, $\sigma_{\varphi_m}|_{\tau_k=0}$, are obtained for all combinations of

m	h_{tm}	$p_t p_r$	$\bar{\varphi}_m$ [$^\circ$]	σ_{φ_m} [$^\circ$]	$\bar{\tau}_m$[ns]	σ_{τ_m}[ns]
1	15	VV	0.6	16.6	1.8	3.6
1	15	HV	5.6	17.6	3.7	7.9
1	15	VH	1.2	10.3	1.1	0.7
1	15	HH	1.3	9.0	1.0	0.4
2	12	VV	13.8	13.8	8.7	13.2
2	12	HV	13.6	22.3	19.9	15.7
2	12	VH	17.8	13.8	8.6	13.8
2	12	HH	1.8	12.4	1.7	3.3
3	9	VV	-0.3	10.8	1.1	0.5
3	9	HV	10.6	6.7	1.2	2.0
3	9	VH	8.7	13.1	2.3	5.9
3	9	HH	5.0	8.4	1.0	0.3
3	6	VV	7.0	9.0	1.0	0.3
4	6	HV	-0.8	5.7	1.0	0.2
4	6	VH	11.2	9.6	1.4	3.5
4	6	HH	-5.7	6.6	1.3	0.6
5	4	VV	0.4	10.4	1.0	0.3
5	4	HV	3.0	17.5	1.6	1.5
5	4	VH	5.7	22.1	1.2	1.4
5	4	HH	-0.7	5.1	1.0	0.1

Table 2. Radio Signal Spread Estimated Moments

transmitter antenna height h_{tm} and transmitter-receiver polarizations $p_t p_r$ are presented in Table 2. Considering the delay resolution of the measurement, 20 [ns], the small values for the standard deviation of excess-delay σ_τ agrees with the previously reported results. This is because the dispersion is caused due to scatterings by leaves and branches along the propagation path.

To get a sense of azimuth standard deviations it is necessary to obtain the azimuth resolution for the current analysis. Figure 4 shows the Capon spectrum for a single path measured in the anechoic chamber. While the Rayleigh resolution is slightly larger than the theoretical value 11.5° it shall not be confused with the resolution of the standard deviation. The computed standard deviation for the Capon spectrum of Fig. 4 is $\sigma_\varphi = 4.8^\circ$. This means any deviation larger than this value is caused by the dispersion of the radio wave while propagating through foliage.

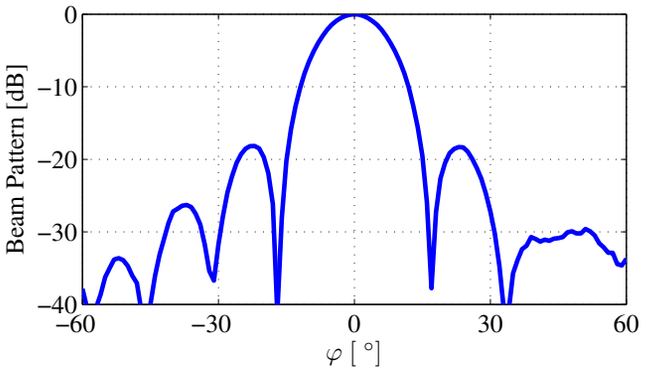

Figure 4. Capon spectrum of a single path in the azimuth.

3.2. Multipath cluster identification –high-resolution analysis

A simple manual cluster identification algorithm was applied to the estimated multipath. As the purpose is to identify dominant propagation mechanisms, only those clusters conveying significant power are discussed. Each cluster carries a total power calculated as

$$g_{m,c} = \sum_{l \in \mathrm{C}_{m,c}} g_l, \qquad \begin{matrix} m = 1, \cdots, M \\ c = 1, \cdots, C \end{matrix}, \tag{15}$$

where $g_l = |\alpha_l|^2$ is the estimated path-gain, M indicates the number of measurements, C is the number of identified clusters and $\mathrm{C}_{m,c}$ represents the set of estimated mutilpath in cth cluster of measurement m . The mean and standard deviation of the estimated parameters for each cluster can be obtained as

$$\bar{x}_{m,c} = \frac{\sum_{l \in \mathrm{C}_{m,c}} g_l x_l}{g_{m,c}}, \qquad \begin{matrix} m = 1, \cdots, M \\ c = 1, \cdots, C \end{matrix}, \tag{16}$$

$$\sigma_{x_{m,c}} = \left(\frac{\sum_{l \in \mathrm{C}_{m,c}} (x_l - \bar{x}_{m,c}) g_l}{g_{m,c}} \right)^{1/2}, \qquad \begin{matrix} m = 1, \cdots, M \\ c = 1, \cdots, C \end{matrix}. \tag{17}$$

Here x is a substitute variable for the estimated path parameters except for the path magnitude, i.e. $x \in \{\tau, \varphi_\mathrm{r}, \vartheta_\mathrm{r}\}$.

Table 3 displays most significant clusters identified for each measurement. In this table different number of clusters are presented for each measurement with the specifications of the measurement such as the measurement index m, transmitter antenna height $h_{\mathrm{t}m}$, polarizations of transmit and received signal $p_\mathrm{t} p_\mathrm{r}$ and receive signal noise level σ_n^2; as well the specifications of the clusters are exhibited as the index of the cluster for each measurement c, number of multipath in the cluster $L_{m,c}$, cluster's associated power $g_{m,c}$ followed the average and standard deviation of excess-delay, azimuth- and elevation-of arrival of the cluster.

One observation is that significant clusters are of mixed polarization combinations, that is the channel acts random interactions with the radio wave in terms of polarization. Also notable is that there could be found almost no significant cluster associated with back scattering. Moreover it is observed that for the measurement number 2 with the transmit antenna height of $h_{\mathrm{t}2} = 12$ [m] the received signal is weaker compared to other measurements. Hence the number of estimated multipath as well as identified clusters are smaller. In the next

subsection these strictly identified clusters are grouped to recognize what we call propagation mechanisms.

3.3. Propagation mechanisms –high-resolution analysis

With the strict classification of multipath in the previous section we have derived clusters in the Table 3 which can not be so informative when it comes to the propagation mechanism analysis. In this section those clusters are further arranged in groups of related clusters to provide a better knowledge of the channel. Here we are specifically interested in clusters with close mean angle-of-arrival ($\bar{\varphi}_{m,c}$, $\bar{\vartheta}_{m,c}$) to identify propagation mechanisms in the channel. It is observed that clusters with different excess-delays could exist in the same group, hence those clusters belonging to the same group may not represent identical propagation mechanism in the strict sense, e.g. both multiple-scattering and single-scattering multipath could be included in the same group, but as long as we are interested in the final interaction of the propagation wave in the channel the current approach suits. As an example consider clusters $C_{1,1}$, $C_{1,4}$, $C_{1,5}$, clearly their close mean angle-of-arrival values hint their last interaction to the channel coming from the same source. By rearrangement of the clusters in such groups within each measurement, we further examined any existing link between these groups among all measurements and found the following classes of received multipath:

A. The foliage close to the receiver in the direction of transmitter scatters a great amount of radio energy. The clusters with a mean azimuth-of-arrival value in the interval $\bar{\varphi}_{m,c} \in (-6^\circ, 10^\circ)$ and with a slight positive elevation-of-arrival belong to this class. This class includes clusters $C_{1,1}$, $C_{1,4}$, $C_{1,5}$, $C_{2,2}$, $C_{3,1}$, $C_{3,2}$, $C_{3,4}$, $C_{3,6}$, $C_{4,1}$, $C_{4,2}$, $C_{4,4}$, $C_{4,7}$, $C_{4,8}$, $C_{4,11}$, $C_{5,1}$, $C_{5,3}$, $C_{5,5}$, $C_{5,15}$.
B. Scattering from the foliage close to the receiver and with azimuth-of-arrival values in the interval $\bar{\varphi}_{m,c} \in (17^\circ, 30^\circ)$ and with slight positive values of elevation-of-arrival can be associated to this class. Clusters in this class are $C_{1,2}$, $C_{1,3}$, $C_{1,6}$, $C_{1,8}$, $C_{1,9}$, $C_{2,1}$, $C_{2,3}$, $C_{3,3}$, $C_{3,5}$, $C_{3,7}$, $C_{4,3}$, $C_{4,9}$, $C_{4,10}$, $C_{5,6}$, $C_{5,9}$, $C_{5,10}$.
C. Third class of identified clusters represents the foliage located in the azimuth-of-arrival in the interval $\bar{\varphi}_{m,c} \in (-40^\circ, -16^\circ)$ and again with slight positive values of elevation-of-arrival. This class of clusters include $C_{1,11}$, $C_{3,9}$, $C_{4,5}$, $C_{4,6}$, $C_{5,2}$, $C_{5,7}$, $C_{5,14}$.

Few clusters remain unclassified conveying minor radio energy compared to these three classes of clusters. It is important to remember that this classification was done among different measurements particularly in terms of transmitter antenna heights. Figure 5 schematically illustrates top view of the radio channel and three major classes of identified clusters. It can be said that major propagation mechanisms in this channel are associated with one of these classes. Class A represents the forward scattering component. Even though there is no line-of-sight from the foliage to the transmitter in any of the measurements, this class introduces the most powerful propagation mechanism in the channel. The radio signal finds its way through the leaves and in between tree trunks to reach to this foliage and be rescattered toward the receiver. It is observed that strongest clusters in all measurements, except measurement 2, are put in this class.

To describe the scatterings from classes B and C it is noticed that even though the measurement area is densely vegetated, the density of foliage is not homogeneous

m	$h_{\mathrm{t}m}$	$p_{\mathrm{t}}p_{\mathrm{r}}$	σ_{n}^2 [dB]	c	$L_{m,c}$	$g_{m,c}$ [dB]	$\bar{\tau}_{m,c}$ [ns]	$\sigma_{\tau m,c}$ [ns]	$\bar{\varphi}_{m,c}$ [°]	$\sigma_{\varphi m,c}$ [°]	$\bar{\vartheta}_{m,c}$ [°]	$\sigma_{\vartheta m,c}$ [°]
1	15	VV	3.6	1	12	73.8	20	13.1	-3	3.9	26	12.2
1	15	VV	3.6	2	6	49.3	20	10.4	27	6.1	9	9.9
1	15	HH	3.9	3	2	48.7	20	4.9	23	0.0	1	0.0
1	15	HV	3.8	4	1	48.1	0	0.0	-6	0.0	26	0.0
1	15	VH	3.6	5	3	45.6	20	12.7	-1	1.4	12	2.5
1	15	VV	3.6	6	1	38.3	60	0.0	28	0.0	3	0.0
1	15	HH	3.9	7	1	37.4	40	0.0	-139	0.0	1	0.0
1	15	VH	3.6	8	3	34.4	40	10.0	27	5.0	6	10.3
1	15	HV	3.8	9	2	34.3	0	9.8	24	0.5	13	7.8
2	12	VV	2.6	1	5	50.4	40	10.0	17	7.9	2	3.8
2	12	VV	2.6	2	1	32.4	0	0.0	-1	0.0	19	0.0
2	12	HV	2.7	3	2	27.5	20	4.5	19	6.3	1	0.0
3	9	HV	2.4	1	11	65.0	20	9.6	-3	6.8	6	9.0
3	9	VH	2.5	2	2	57.8	20	0.0	5	6.7	11	0.0
3	9	HV	2.4	3	4	55.9	40	11.8	23	5.6	3	0.8
3	9	VH	2.5	4	3	45.5	40	8.7	10	0.9	11	0.0
3	9	HV	2.4	5	2	43.7	0	4.6	23	2.3	7	9.6
3	9	HV	2.4	6	5	45.5	60	7.8	1	3.8	2	5.2
3	9	HV	2.4	7	2	34.6	80	5.0	21	1.0	1	0.0
3	9	HV	2.4	8	2	34.5	60	8.5	-60	5.1	3	0.0
4	6	HH	2.6	1	7	70.6	20	8.3	-2	4.6	8	6.5
4	6	VV	2.4	2	4	64.5	0	8.8	8	7.5	3	1.5
4	6	HH	2.6	3	4	60.2	40	7.5	19	5.5	2	3.1
4	6	HV	2.4	4	3	54.2	20	8.5	-6	3.4	1	0.5
4	6	VV	2.4	5	2	49.4	0	7.6	-16	5.3	10	9.8
4	6	VV	2.4	6	5	48.0	40	14.2	-40	7.7	1	5.2
4	6	HH	2.6	7	3	42.9	100	5.0	-2	1.3	11	0.0
4	6	VV	2.4	8	3	42.5	60	5.0	5	2.6	1	0.0
4	6	VH	2.4	9	2	42.5	0	4.6	19	0.5	5	0.0
4	6	HH	2.6	10	1	41.0	20	0.0	30	0.0	5	0.0
4	6	HH	2.6	11	4	40.8	60	9.1	0	5.6	11	0.0
5	4	VV	2.8	1	10	77.3	20	8.0	0	5.1	9	3.6
5	4	VV	2.8	2	4	57.6	20	4.8	-29	2.0	30	7.4
5	4	HV	2.6	3	6	57.5	20	4.6	1	8.6	29	5.9
5	4	VV	2.8	4	3	54.2	20	0.0	-101	2.7	32	1.7

Table 3. Identified Clusters

m	h_{tm}	$p_t p_r$	σ_n^2 [dB]	c	$L_{m,c}$	$g_{m,c}$ [dB]	$\bar{\tau}_{m,c}$ [ns]	$\sigma_{\tau m,c}$ [ns]	$\bar{\varphi}_{m,c}$ [°]	$\sigma_{\varphi m,c}$ [°]	$\bar{\vartheta}_{m,c}$ [°]	$\sigma_{\vartheta m,c}$ [°]
5	4	HH	2.7	5	2	53.8	40	0.0	1	3.7	13	4.5
5	4	VV	2.8	6	3	50.4	20	8.7	27	3.2	9	2.5
5	4	HH	2.7	7	3	46.5	40	9.5	-28	5.6	20	4.2
5	4	VV	2.8	8	3	43.8	20	0.0	145	7.4	5	2.0
5	4	HH	2.7	9	3	40.2	40	9.3	34	5.8	9	3.4
5	4	VV	2.8	10	2	38.8	80	9.3	20	0.9	5	1.4
5	4	VV	2.8	11	2	36.8	20	0.0	98	5.9	7	0.5
5	4	VV	2.8	12	3	36.6	20	8.7	46	3.1	33	9.8
5	4	HH	2.7	13	1	35.4	60	0.0	3	0.0	-40	0.0
5	4	HV	2.6	14	2	35.2	20	7.7	-18	0.8	28	8.4
5	4	VH	2.8	15	3	34.3	20	9.7	0	4.6	17	4.5
5	4	VV	2.8	16	2	33.9	40	0.0	-98	4.4	29	4.4

Table 3. Identified Clusters *(Continued).*

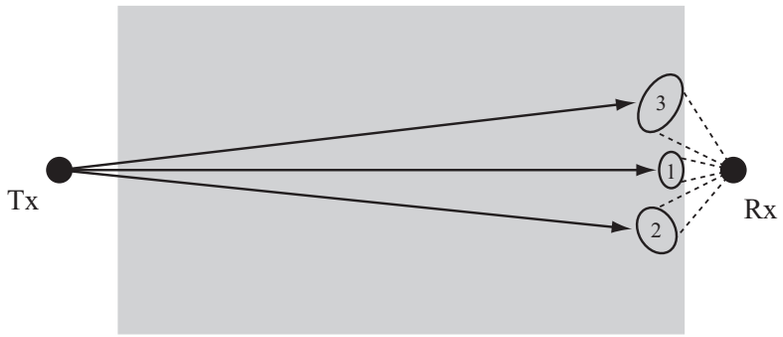

Figure 5. Schematic top view of the radio channel and three major classes of received multipath. No line-of-sight exists between transmitter and antenna and these classes.

everywhere. This produces airy spaces within the dense vegetation which act similar to canyons to conduct radio signals. Figure 6 displays such spaces in the vegetation viewed from the measurement 4 transmitter antenna position, $h_{t4} = 6$ [m]. When these guided signals arrive to one or more foliage with line-of-sight toward the receiver they make strong clusters of received propagation waves. It seems this is what happens in case of multipath classes B and C. Notable is that strong clusters from measurements with higher transmit antenna contribute to class B whereas those from measurements with lower antenna height, e.g. measurement 5, appear strongly in class C.

Again it is reminded that there is not any line-of-sight from the transmitter to the foliages associated with any of classes, however the configuration of foliage within the vegetation area causes the radio signal to be nonuniformly received in format of clusters. The significant point in the classification process is that clusters from every transmitter height, and from a variety of polarization combinations are taking part in each multipath class. The interpretation can be that even if the interactions of multipath to the vegetation is of random nature and number, when it comes to the angle-of-arrival the receiving radio signal can be from a deterministic selected number of directions.

Figure 6. Airy spaces within dense vegetated area. Viewed from transmitter antenna location at $h_{t4} = 6$ [m].

4. Discussion

Typical measurements for the analysis of the interaction between radio waves and vegetation, as well to evaluate the existing models, generally target only the field attenuation along distance. Moreover, measurement schemes and facilities usually do not acquire enough resolution to support an accurate analysis of the active mechanisms and basically provide limited insight into the physical phenomena which in reality is complex. There are nearly universal assumptions, e.g. vegetation as a homogeneous media of randomly distributed scatterers, used in most corresponding studies which have never been evaluated. In this chapter the directional radio channel in dense vegetation is investigated through the analysis of appropriate measurement data. Two different analysis methods are used for the comparison of results.

First the dispersions in delay and azimuth-of-arrival of the received waves are derived by using a beam-forming. Investigating the mean delay values in the Table 2 shows that in some cases components other than the direct path have been involved in the analysis. The interpretation of some large spreads in azimuth and the distance of the mean azimuth values from zero shall be related to this fact. The main conclusion of the analysis however is to confirm the received signal spatial spread due to interaction with foliage, and to provide rough estimates of this spread. It is observed that even though the beam-forming approach is robust, easy to implement and does not require any presumption regarding the received signal, its spatial resolution proves limited. Hence the received signal energy through different propagation mechanisms can not be accurately separated. Moreover the array antenna response is included in the channel and can not be de-embedded.

For the propagation mechanisms to be distinguished, high resolution parameter estimation of the measured data is necessary. The well known SAGE algorithm is used to identify received propagation multipath, which are then grouped in clusters using a simple clustering algorithm. Specifically looking at the measured receiving radio signal with high resolution in angular domain, three major classes of received multipath associated with separate final scattering foliage are identified. Thus contrary to the widely assumed homogeneous

random scattering media it was observed that the radio waves in the vegetated channel are received from distinct directions in clusters of multipath. The identified classes of multipath correspond to two significant propagation mechanisms other than forward scattering by the foliage obstructing the line-of-sight –normally used as the main mechanism in different approaches. It seems airy spaces in the vegetated area can have crucial influence in directing the radio signal toward specific directions, to be redirected to the receiver by a foliage with the line-of-sight toward the receiver.

The significant point is that by beam-forming analysis of the measurement data it is not possible to identify those propagation mechanisms, although limited insight regarding the spatial spread of the direct received path achieved. Thus appropriate measurements assisted with high-resolution data analysis can meaningfully change our understanding of the vegetation wireless channel and substantially modify corresponding models.

It is now well known that in most practical wireless channels the diffuse scattering plays a considerable role in terms of carrying the radio energy [52],[53]. In comparison to the specular component, the estimation and modeling of which is rather straightforward, the estimation and modeling of the diffuse component can be rather complicated. Nevertheless, due to the random shape and direction of trees and branches in any foliage, it is expected that a major part of energy is transferred by means of diffuse component. Further high-resolution investigation and modeling of the radio channel including the diffuse component is left as a future task.

5. Conclusion

In this chapter the radio channel in dense vegetation is investigated through the directional analysis of carefully gathered measurement data. By looking at the measured receiving radio signal with high resolution in angular domain, three major classes of received multipath associated with separate final scattering foliage are identified. The identified classes of multipath correspond to two significant propagation mechanisms other than forward scattering by the foliage obstructing the line-of-sight which is normally considered as the main mechanism in such channels. The airy spaces in the vegetated area is probably accounted for directing the radio signal toward specific directions. These are redirected toward the receiver by a foliage in its line-of-sight. Thus contrary to the widely assumed homogeneous random scattering media it was observed that the radio waves in the vegetated channel are received from distinct directions in clusters of multipath. Results of the high-resolution analysis are in contrast to the beam-forming analysis of the measured data which is also presented in the chapter for comparison. This proves that state-of-the-art measurements assisted with high-resolution analysis can modify our understanding and modelings of the phenomena. Moreover to fully analyze and understand these channels, the diffuse component also has to be estimated and modeled which is left as a future task.

Author details

Mir Ghoraishi
Tokyo Institute of Technology, Japan,
University of Surrey, United Kingdom

Jun-ichi Takada
Tokyo Institute of Technology, Japan

Tetsuro Imai
NTT DOCOMO Inc., Kanagawa, Japan

6. References

[1] M. Weissberger, "An initial critical summary of models for predicting the attenuation of radio waves by trees," ESD-TR-81-101, EMC Analysis Center, Annapolis MD, USA, 1982.
[2] COST 235, Radiowave propagation effects on next generation fixed services terrestrial telecommunications systems, Final Report, ISBN 92-827-8023-6, Commission of the European Union, 1996.
[3] F. Schwering, E. Violette, R. Espeland, "Millimeter-wave propagation in vegetation: Experiments and theory," *IEEE Trans. Geoscience and Remote Sensing*, Vol. 26, pp. 355Ű367, May 1984.
[4] R. Tewari, S. Swarup, M. Roy, "Radio wave propagation through rain forests of india," *IEEE Trans. Antennas and Propagation*, Vol. 38, No. 4, pp. 433Ű449, Apr. 1990.
[5] M. Al-Nuaimi, A. Hammoudeh, "Attenuation functions of microwave signals propagated through trees," *Electronics Letters*, Vol. 29, No. 14, pp. 1307-1308, July 1993.
[6] A. Seville, "Vegetation attenuation: modelling and measurements at millimetric frequencies," *Int. Conf. Antennas and Propagation*, Vol. 2, pp.5-8, April 1997.
[7] M. Al-Nuaimi, A. Hammoudeh, "Measurements and predictions of attenuation and scatter of microwave signals by trees," *IEE Proc. Microwaves, Antennas and Propagation*, Vol. 141, No. 2, pp. 70-76, April 1994.
[8] R. Stephens, M. Al-Nuaimi, R. Calderinha, "Characterisation of depolarization of radio signals by single trees at 20 GHz," *Fifteenth National Radio Science Conference (URSI)*, B12, 1-7, Feb. 1998.
[9] T. Tamir, "On radio-wave propagation in forest environments," *IEEE Trans. Antennas and Propagation*, Vol. 15, No. 6, pp. 806-817, Nov. 1967.
[10] L. Li, J. Koh, T. Yeo, M. Leong, P. Kooi, "Analysis of radiowave propagation in a four-layered anisotropic forest environment," *IEEE Trans. Geoscience and Remote Sensing*, Vol. 37, No. 4, pp. 1967-1979, July 1999.
[11] G. Cavalcante, D. Rogers, A. Giardola, "Radio loss in forests using a model with four layered media," *Radio Science*, Vol. 18, 1983.
[12] L. Li, T. Yeo, P. Kooi, M. Leong, "Radio wave propagation along mixed paths through a four-layered model of rain forest: an analytic approach," *IEEE Trans. Antennas and Propagation*, Vol. 46, No. 7, pp. 1098-1111, July 1998.
[13] Y. de Jong, M. Herben, "A tree-scattering model for improved propagation prediction in urban microcells," *IEEE Trans. Vehicular Technology,* vol. 53, pp. 503.513, Mar. 2004.
[14] A. H. Lagrone, "Propagation of VHF and UHF electromagnetic waves over a grove of trees in full leaf," *IEEE Trans. Antenna and Propagation,* Vol. 25, pp. 866-869, Nov. 1977.
[15] R. Matschek, B. Linot, H. Sizun, "Model for wave propagation in presence of vegetation based on the UTD associating transmitted and lateral waves," *Proc. IEE National Conf. Antennas and Propagation*, pp. 120-123, April 1999.

[16] F. Schubert, B. Fleury, P. Robertson, R. Prieto-Cerdeira, A. Steingass, A. Lehner, "Modeling of Multipath Propagation Caused by Trees and Its Effect on GNSS Receiver Performance," *European Conf. Antennas and Propagation (EUCAP 2010),* 2010.
[17] A. Ishimaru, *Wave Propagation and Scattering in Random Media*, Academic Press, 1978.
[18] L. Tsang, J. Kong, K. Ding, C. Ao, *Scattering of Electromagnetic Waves*, Wiley, 2001.
[19] S. Saatchi, K. McDonald, "Coherent effects in microwave backscattering models for forest canopies," *IEEE Trans. Geoscience and Remote Sensing*, Vol. 35, No. 4, July 1997.
[20] R. Johnson, F. Schwering, "A Transport Theory of Millimeter Wave Propagation in Woods and Forests," Research and Development Technical Report, CECOM-TR-85-1, Feb. 1985
[21] D. Didascalou, M. Younis, W. Wiesbeck, "Millimeter-wave scattering and penetration in isolated vegetation structures," *IEEE Trans. Geoscience and Remote Sensing*, Vol. 38, pp. 2106Ű2113, Sep. 2000.
[22] T. Fernandes, R. Caldeirinha, M. Al-Nuaimi, J. Richter, "A discrete RET model for millimeter-wave propagation in isolate tree formations," *IEICE Trans. Communications*, Vol. E88-B, No. 6, pp. 2411Ű2418, Jun. 2005.
[23] L. Foldy, "The multiple scattering of waves," *Physical Review*, Vol. 67, No. 3, pp. 107-119, 1945.
[24] L. Li, J. Koh, T. Yeo, M. Leong, P. Kooi, "Analysis of radiowave propagation in a four-layered anisotropic forest environment," *IEEE Trans. Geoscience and Remote Sensing*, Vol. 37, No. 4, pp. 1967-1979, July 1999.
[25] Y. Lin, K. Sarabandi, "A Monte Carlo coherent scattering model for forest canopies using fractal-generated trees," *IEEE Trans. Geoscience and Remote Sensing*, Vol. 37, pp. 440Ű451, 1999.
[26] Y. Lin, K. Sarabandi, "Retrieval of forest parameters using a fractal-based coherent scattering model and a genetic algorithm," *IEEE Trans. Geoscience and Remote Sensing*, Vol. 37, pp. 1415Ű1424, May 1999.
[27] I. Koh, K. Sarabandi, "Polarimetric channel characterization of foliage for performance assessment of GPS receivers under tree canopies," *IEEE Trans. Antennas and Propagation,* Vol. 50, No. 5, pp. 713Ű72, 2002.
[28] I. Koh, F. Wang, K. Sarabandi, "Estimation of coherent field attenuation through dense foliage including multiple-scattering, *IEE Trans. Geoscience and Remote Sensing,* Vol. 41, pp. 1132Ű1135, 2003.
[29] F. Wang, K. Sarabandi, "An enhanced millimeter-wave foliage propagation model," *IEEE Trans. Antennas and Propagation,* Vol. 53, No. 7, pp. 2138Ű2145, Jul. 2005.
[30] F. Wang, K. Sarabandi, "A Physics-Based Statistical Model for Wave Propagation Through Foliage," *IEEE Trans. Antennas and Propagation,* Vol. 55, No. 3, Part 2, pp. 958-968, March 2007.
[31] S. Torrico, H. Bertoni, R. Lang, "Modeling tree effects on path loss in a residential environment," *IEEE Trans. Antennas and Propagation*, Vol. 46, No. 6, pp. 872-880, June 1998.
[32] S. Torrico, R. Lang, "A Simplified Analytical Model to Predict the Specific Attenuation of a Tree Canopy," *IEEE Trans. Vehicular Technology*, Vol. 56, No. 2, pp. 696-703, March 2007.
[33] N. Blaunstein, I. Kovacs, Y. Ben-Shimol, J. Andersen, D. Katz, P. Eggers, R. Giladi, K. Olesen, "Prediction of UHF path loss for forest environments," *Radio Science*, Vol. 38, No. 3, 2003.

[34] N. Blaunstein, D. Censor, D. Katz, "Radio propagation in rural residential areas with vegetation," *Progress in Electromagnetic Research*, PIER 40, pp. 131-153, 2003.
[35] N. Rogers, A. Seville, J. Richter, D. Ndzi, N. Savage, R. Caldeirinha, A. Shukla, M. Al-Nuaimi, K. Craig, E. Vilar, J. Austin, A generic model of 1-62 Ghz radio attenuation in vegetation - Final report, Available On-line.
[36] ITU-R Recommendation P.527-3, 1978-1982-1990-1992-2000.
[37] ITU-R Recommendation P.833-4, Oct. 11, 2004.
[38] R. Lewenz, "Path loss variation due to vegetation movement," *Proc. IEE National Conf. Antennas and Propagation*, pp. 97-100, April 1999.
[39] M. Hashim, S. Stavrou, "Measurements and modeling of wind influence on radio wave propagation through vegetation," *IEEE Trans. Wireless Communications,* vol. 5, pp. 1055-1064, May 2006.
[40] Y. Lee, Y. Meng, "Tropical weather effects on foliage propagation," *European Conf. Antennas and Propagation (EuCAP2007),* Nov. 2007.
[41] D. Ndzi, N. Savage, K. Stuart, "Wideband Signal propagation through Vegetation," XVII GA of URSI, Oct. 2005.
[42] Y. Meng, Y. Lee, B. Ng, "Study of the diversity reception in a forested environment," IEEE Trans. Wireless Communications, Vol. 8, No. 5, pp. 2302-2305, May 2009.
[43] M. Gans, N. Amitay, Y. Yeh, T. Damen, R. Valenzuela, C. Cheon, J. Lee, "Propagation measurements for fixed wireless loop (FWL) in a suburban region with foliage and terrain blockages," *IEEE Trans. Wireless Communications,* Vol. 1, pp. 302-310, Apr. 2002.
[44] G. Joshi, C. Dietrich, C. Anderson, W. Newhall, W. Davis, J. Isaacs, G. Barnett, "Near-ground channel measurements over line of sight and forested paths," *IEE Proc. Antennas and Propagation,* Vol. 152, pp. 589-596, Dec. 2005.
[45] C. Oestges, B. Villacieros, D. Vanhoenacker-Janvier, "Radio Channel Characterization for Moderate Antenna Heights in Forest Areas ," *IEEE Trans. Vehicular Technology*, Vol. 58, No. 8, pp. 4031-4035, Oct. 2009.
[46] M. Ghoraishi, J. Takada, C. Phakasoum, T. Imai, K. Kitao, "Azimuth and Delay Dispersion of Mobile Radio Wave Propagation through Vegetation," *European Conf. Antennas and Propagation (EuCAP 2010),* April 2010.
[47] Mir Ghoraishi, Jun-ichi Takada, Tetsuro Imai, "Analysis of Radio Wave Dispersion Through Vegetation," *European Conf. Antennas and Propagation (EuCAP 2012),* March 2012.
[48] X. Yin, *High-Resolution Parameter Estimation for MIMO Channel Sounding,* PhD Thesis, Aalborg University, July 2006.
[49] H. Van Trees, *Optimum Array Processing,* Wiley-Interscience, 2002.
[50] M. Tapio, "On the use of beamforming for estimation of spatially distributed signals," *IEEE Conf. Acoustics, Speech, Signal Processing (ICASSP),* Vol. V, pp. 369-372, 2003.
[51] B. Fleury, M. Tschudin, R. Heddergott, D. Dahlhaus, K. Pedersen, "Channel Parameter Estimation in Mobile Radio Environments Using the SAGE Algorithm," *IEEE J. Selected Areas in Communications*, Vol. 17, No. 3, pp. 434-450, March 1999.
[52] A. Richter, R. Thoma, "Joint Maximum Likelihood Estimation of Specular Paths and Distributed Diffuse Scattering," *IEEE Vehicular Technology Conf. (VTC05-Spring),* Vol. 1, pp. 11-15, June 2005.
[53] F. Mani, C. Oestges, "Evaluation of Diffuse Scattering Contribution for Delay Spread and Crosspolarization Ratio Prediction in an Indoor Scenario," *European Conf. Antennas and Propagation (EuCAP 2010),* April 2009.